

DNA Electrophoresis Studied with the Cage Model

A. van Heukelum,* G. T. Barkema,* and R. H. Bisseling†

**Institute for Theoretical Physics, Utrecht University, Leuvenlaan 4, 3584 CE Utrecht, The Netherlands;*
and †*Mathematical Institute, Utrecht University, P.O. Box 80010, 3508 TA Utrecht, The Netherlands*
E-mail: heukelum@phys.uu.nl

Received February 5, 2001; revised November 5, 2001

The cage model for polymer reptation, proposed by Evans and Edwards, and its recent extension to model DNA electrophoresis are studied by numerically exact computation of the drift velocities for polymers with a length L of up to 15 monomers. The computations show the Nernst–Einstein regime ($v \sim E$) followed by a regime where the velocity decreases exponentially with the applied electric field strength. In agreement with de Gennes’ reptation arguments, we find that asymptotically for large polymers the diffusion coefficient D decreases quadratically with polymer length; for the cage model, the proportionality coefficient is $DL^2 = 0.175(2)$. Additionally we find that the leading correction term for finite polymer lengths scales as $N^{-1/2}$, where $N = L - 1$ is the number of bonds. © 2002 Elsevier Science (USA)

I. INTRODUCTION

In the rapidly growing field of molecular genetics and genetic engineering, gel electrophoresis is a technique of great importance. One reason is that it enables efficient separation of polymer strands by length. In DNA electrophoresis, strands of DNA of various lengths are injected into a gel composed of agarose and a buffer solution. Since DNA is acidic, it becomes negatively charged. Next, an electric field is applied which causes the DNA to migrate in one direction. Since shorter strands travel faster than longer ones, the initial mixture of strands will become separated, allowing the measurement of the relative concentrations of strands of different lengths, or the isolation of strands with a particular length. Given the great practical importance of DNA electrophoresis, there is much interest in gaining an understanding of precisely what the mechanisms of gel electrophoresis are and how the migration rate depends on strand length, applied electric field and the properties of the agarose gel.

It is known that in the gel, agarose forms long strands which cross-link and impede movement of the polymer transverse to its length; its movement is dominated by a mechanism

which de Gennes [1] has dubbed *reptation*: movement of a polymer along its own length by diffusion of stored length.

A commonly used lattice model to simulate the dynamics of reptation is the so-called “repton model,” introduced by Rubinstein in 1987 [2]. Rubinstein had already conjectured that the diffusion coefficient D as a function of polymer length L for long polymers is given by $DL^2 = 1/3$ (with large finite-size effects); this conjecture was further corroborated by van Leeuwen and Kooiman [3–5], and finally proven by Prähofer and Spohn [6]. The repton model has been extended to study electrophoresis by Duke [7–9], and the resulting model—known as the Duke–Rubinstein model—has been studied numerically and analytically by several groups [10–14] and compared to experiments [15].

The main findings of these studies are that the property $DL^2 = 1/3$ (with large finite-size effects) in combination with the fluctuation–dissipation theorem results in a drift velocity $v \sim E/L$ for small electric field strength E , and that for some value of $E \sim 1/L$ this regime crosses over in a regime where the drift velocity ceases to be length dependent and is given by $v \sim E^2$, the so-called *plateau mobility* regime. Furthermore, it was found to be a property of the model in the limit of large E , that the drift velocity decays exponentially, $v \sim e^{(2-L)E/2}$ and $v \sim e^{(3-L)E/2}$ for even and odd L , respectively [16].

Before the introduction of the repton model, Evans and Edwards had introduced the so-called “cage model” to simulate the dynamics of reptation [17]. Also in this model, DL^2 approaches a constant in the limit of large chains [18], which in combination with the fluctuation–dissipation theorem leads to $v \sim E/L$ for small electric field strengths. This model has recently been extended to electrophoresis and studied with Monte Carlo simulations [19]. Besides the expected fluctuation–dissipation regime, these simulations also featured the plateau mobility regime where $v \sim E^2$; these are the two regimes that were identified for the Duke–Rubinstein model using Monte Carlo simulations. Additionally, a third regime was reported where v decreases with increasing E .

This article presents numerically exact computations on the cage model, extended for electrophoresis as in Ref. [19]. As in most models, numerically exact results can only be obtained for relatively small systems (here, for polymers up to a length of $L = 15$), but they do not have the inherently large statistical errors of Monte Carlo results. Thus, they allow for a different class of analysis techniques, for instance those exploiting numerical differentiation. The combination of numerically exact results for short chains with the Monte Carlo results for larger chains reported in Refs. [18, 19] provides a more complete picture of the model.

The calculations done in this work, with a chain length of up to $L = 15$, are computationally challenging and could only be obtained by the exploitation of symmetries in the model, combined with the application of parallel processing. The state vector of the cage model for electrophoresis has 6^{L-1} components, and the original transition matrix which represents the transition probabilities between polymer configurations is of size $6^{L-1} \times 6^{L-1}$ (see Section II). We show that many components of the steady-state vector are equal, because the configurations they belong to are equivalent. By using those equivalences, the original transition matrix could be reduced significantly (see Section III). The parallel implementation of the computation is done by spreading the nonzeros of the sparse transition matrix over the processors. Interprocessor communication is reduced by exploiting the specific sparsity structure of the matrix (see Section IV). The combined effect of decreasing the matrix size, improving the eigenspectrum of the matrix,

and applying parallel processing accelerates the computation by more than a factor of a million, allowing us to reach larger values of L ; in this paper we present numerically exact values for the diffusion coefficients for polymers up to length $L = 15$ (see Section V). We also present computation times and parallel efficiency results for up to 64 processors of a Cray T3E computer (see Section VI). The conclusions are summarized in Section VII.

II. CAGE MODEL FOR REPTATION

The cage model, introduced by Evans and Edwards [17], describes a polymer that moves through a gel. The polymer is modeled as a chain of “monomers,” connected by *bonds*. Two monomers connected by a bond must reside in adjacent sites of a cubic lattice. No other excluded volume interactions are enforced, so each lattice site may contain many monomers. Figure 1 shows an impression of the model. The configuration of a cage polymer is most easily defined by the set of directions of all the bonds. The bond representations shown in Fig. 2 are $-y + x + y + y + y - y - y + x - x - y + x$ and $-y + x - x + x - y - y - x + y + x + x - x$. A part of a configuration consisting of a monomer with two opposite bonds is called a *kink*. In the left part of Fig. 2, the configuration features kinks at monomers 5 and 8, and in the right part at monomers 2, 3, and 10.

The gel is modeled by the edges of a cubic lattice, translated by a vector $(\frac{1}{2}, \frac{1}{2}, \frac{1}{2})$ relative to the lattice on which the polymer resides. The dynamics of a cage polymer consists of those single monomer moves for which the polymer does not cut gel strands. This leaves two classes of allowed moves: (i) a kink is randomly replaced by a kink in one of the six possible directions; (ii) a bond at an end monomer is randomly replaced by a bond in one of the six possible directions. Every other single monomer move is forbidden because it would cause the polymer to cross a gel strand. The model does not impose self-avoidance on the polymer chain, which is justified because a typical mixture of long DNA strands is semidilute in electrophoresis experiments, and because for short strands the self-avoidance is negligible since the persistence length of DNA is much larger than its diameter. The diffusion coefficient of the polymer chains can be computed from the displacement of the center of mass [18].

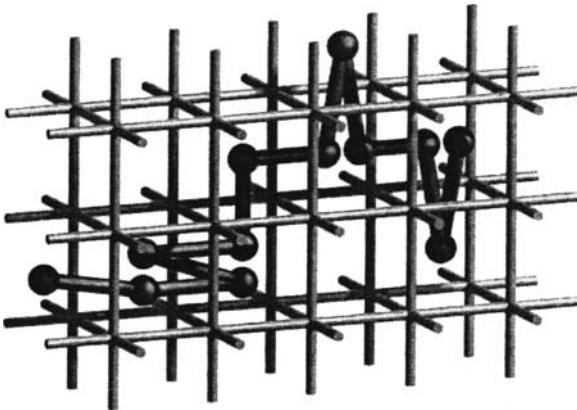


FIG. 1. An impression of the cage model for reptation. The polymer consists of a sequence of monomers, connected by unit-length bonds.

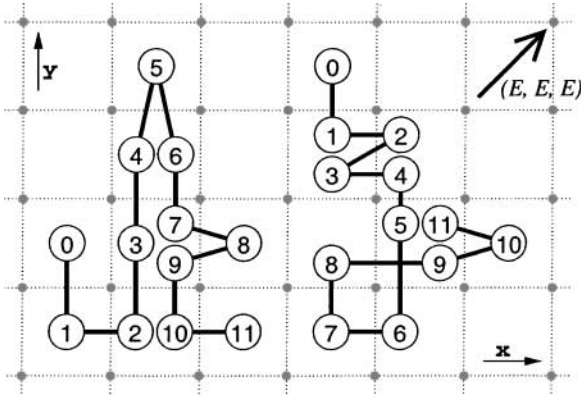


FIG. 2. The cage model. The dotted lines denote the gel strands in the x - y plane, and the large gray dots are the gel strands in the z direction. The space between the gel strands represents the pores of the gel. The polymer is modeled as a chain of monomers; two adjacent monomers reside in nearest-neighbor pores. We denote bonds that are going right, left, up, down, out of the paper, and into the paper by $+x$, $-x$, $+y$, $-y$, $+z$, and $-z$, respectively. The two example configurations were chosen to be planar, for clarity. The electric field vector points diagonally out of the paper.

The cage model has been extended to include the effects of an electric field on the motion of (charged) polymers [19]. The possible transitions are the same, but the rates are different. The electric field is $\vec{E} = (E, E, E)$, such that replacing a kink with one of the three forward-pointing kinks (along the electric field) occurs with rate e^{qE} , and replacing with by one of the three backward-pointing kinks (against the electric field) occurs with rate e^{-qE} , where q is the dimensionless charge of the moved monomer. In the remainder of this paper, we assume that $q = 1$.

The set of all probabilities of the 6^{L-1} possible configurations can be represented by a 6^{L-1} -dimensional vector. The dynamics of the model is then specified by a sparse $6^{L-1} \times 6^{L-1}$ matrix T . The transition matrix T has $[5(\frac{L-2}{6} + 2) + 1]6^{L-1}$ nonzero elements: each polymer has $L - 2$ inner monomers that can move if their bonds are in opposite directions, and two end monomers that can always move; a monomer that can move goes to one of five new positions or the polymer stays unaltered.

If the polymer is moved along the applied field from configuration j to configuration i , then $T_{ij} = \delta t \cdot e^E$. If the polymer is moved against the applied field, $T_{ij} = \delta t \cdot e^{-E}$. The variable δt can be interpreted as the time step in Monte Carlo simulations. The diagonal element T_{ii} is such that the sum of each column is exactly one. An upper bound for the sum of the off-diagonal elements in column j is $\delta t \cdot 3L(e^E + e^{-E})$, because at most L kinks can move, each in at most three forward and three backward directions. We choose $\delta t = (3L(e^E + e^{-E}))^{-1}$, so that all elements in column j are in the range $[0, 1]$. Thus, T_{ij} is the probability of moving from configuration j to i . Because we have a nonzero probability to stay in the same state, $T_{ii} > 0$ holds for all i . This implies $T_{ij} < 1$ for all $i \neq j$. Because end monomers can always move, we also have $T_{ii} < 1$.

The cage model with an applied electric field is ergodic, i.e., every configuration can reach every other configuration in a finite number of steps. The steady-state vector \vec{a} is the eigenvector of T with eigenvalue one (which is the largest eigenvalue), normalized such that $\sum_i a_i = 1$. The drift velocity of the polymer along one of the principal axes is

$$v = \frac{2}{3} \sum_i a_i (b_i e^E - f_i e^{-E}), \quad (1)$$

where b_i is the number of kinks and end monomers of polymer configuration i pointing backward (which can move forward with a rate of e^E), and f_i the number of kinks and end monomers pointing forward. The factor of $2/3$ appears because moves occur along each of the three principal axes, and because each kink move increases or decreases the sum of the coordinates of a configuration by two.

III. EXPLOITING SYMMETRIES OF THE MODEL

In the model that we study here, the electric field is chosen in the $(1, 1, 1)$ direction, and consequently polymer configurations that are related through rotation around the direction $(1, 1, 1)$ are equivalent, i.e., their probability is the same, irrespective of the field strength. Moreover, in many cases it is possible to rotate *part* of the polymer around this direction while preserving this equivalence. If polymer configurations are grouped into classes containing only equivalent polymers, it is sufficient to determine the probability for one polymer configuration per class rather than for all polymer configurations, since by definition the probabilities are equal within a class.

Instead of working in the state space of all polymer configurations, we work in the state space of all equivalence classes. Since equivalence classes can easily contain thousands of configurations, the state space is thus reduced by several orders of magnitude, and a tremendous speedup is obtained. Next, we discuss how to identify whether two polymer configurations are equivalent, and how physical quantities such as the velocity can be computed within this reduced state space of equivalence classes.

To identify which polymer configurations are equivalent, we construct a representation that puts equivalent configurations in the same class. We call part of a configuration between two monomers *removable* if all monomers between them can be removed by repeatedly removing kinks. A kink is removed by deleting the central monomer and the two bonds connected to it, and merging the two monomers adjacent to the central monomer. In the left part of Fig. 2, monomers 4 and 6 are merged when the kink at monomer 5 is removed. If two polymers have the same sequence of forward and backward bonds, and the same set of removable pairs of monomers, they have the same *kink representation*. The construction of such a representation is illustrated in Fig. 3. The kink representation gives a unique number to each symmetry class. We can prove that all polymer configurations with the same kink representation have the same probability in the steady state (see Appendix), and we have verified this explicitly up to $L \leq 9$. Furthermore, the forward/backward symmetry was removed by also computing the kink representation starting at the other end of the polymer, and then using only the one with the lower binary value.

The reduced state space is constructed by computing the kink representation for each polymer configuration and removing the duplicates (in our implementation, by using hashing). During this phase some additional information is stored about each kink representation: each bond representation that introduces a new kink representation is stored along with the kink representation, and the total number of bond representations for each kink representation is recorded. Table I shows the reduction of the configuration space obtained by removing the symmetries. The kink representations are enumerated by sorting them based on their binary value, with the right-most bit the least significant. This ordering has the property that in most cases moves cause only small changes in binary values, e.g., replacing a kink $+x - x$ with $-y + y$ swaps two bond-direction bits; replacing $+x - x$ with $+y - y$ even keeps them

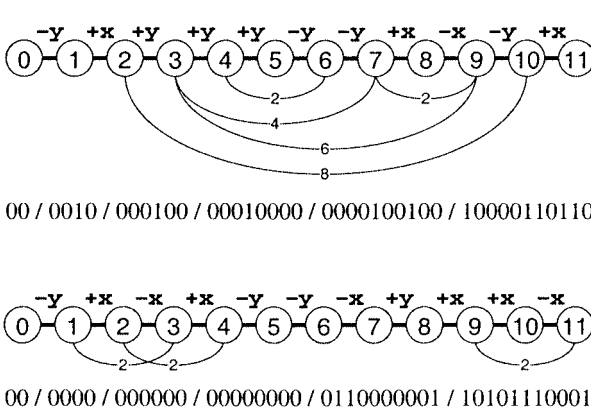


FIG. 3. Kink representations for the two examples from Fig. 2. The arcs show which parts can be removed by repeatedly removing kinks. The kink representations are also given as a binary value; the slashes separate the removable parts of length 10, 8, 6, 4, and 2 and the bond directions. A bit 1 at position r for part length l means that the part between monomers r and $r + l$ can be removed.

the same; the removable-parts bits can be affected as well, but this becomes less likely with increasing part length.

The reduced transition matrix T' is constructed one column at a time. For column j , we consider the possible moves of the bond representation stored with kink representation j . For each resulting bond representation, we compute the associated kink representation i , concluding that kink representation j can move to kink representation i in a single monomer move, and the reduced transition matrix element T'_{ij} is incremented by either $\delta t \cdot e^E$ or $\delta t \cdot e^{-E}$, depending on the direction of the move. Table I shows the resulting reduction factor in the number of nonzero matrix elements. By construction, the matrix T'

TABLE I

The Number of Kink Representations for Polymer Lengths $L = 3$ –15, the Reduction Factor of the State Space, the Number of Nonzero Elements for the Matrix in the Kink Representation, and the Reduction Factor of the Number of Nonzero Elements

| L | Kink representations | Reduction factor | Nonzero elements | Reduction factor |
|-----|----------------------|------------------|------------------|------------------|
| 3 | 5 | 7 | 19 | 22 |
| 4 | 9 | 24 | 49 | 56 |
| 5 | 37 | 35 | 233 | 75 |
| 6 | 93 | 84 | 785 | 142 |
| 7 | 340 | 137 | 3,084 | 229 |
| 8 | 1,015 | 276 | 11,003 | 407 |
| 9 | 3,534 | 475 | 41,594 | 680 |
| 10 | 11,397 | 884 | 150,645 | 1,182 |
| 11 | 39,082 | 1,547 | 559,722 | 1,999 |
| 12 | 130,228 | 2,786 | 2,032,536 | 3,451 |
| 13 | 445,315 | 4,888 | 7,479,343 | 5,869 |
| 14 | 1,505,785 | 8,674 | 27,130,349 | 10,110 |
| 15 | 5,154,859 | 15,202 | 99,199,551 | 17,248 |

has the following properties. The sum of the elements in a column is one. All elements are in the range $[0, 1)$; elements T_{ii} are even in $(0, 1)$. The reduced model is ergodic, and its steady-state vector is the normalized eigenvector with eigenvalue one (which is the largest). The drift velocity is again computed by Eq. (1), where a_i is now the probability of class i , and b_i (f_i) the number of backward (forward)-pointing kinks and end monomers of a single polymer configuration in class i .

Repeatedly multiplying a starting vector by the reduced transition matrix yields the steady-state vector. This iterative method to find the eigenvector of the largest eigenvalue is well-known as the power method, which converges if one eigenvalue is larger in absolute value than all the others. The convergence of the power method depends on the ratio between the largest and the second largest eigenvalue. We can compute the eigenvector faster by applying the power method to $T^{(\omega)} = I + \omega(T' - I)$, which has eigenvalues $\lambda_i^{(\omega)} = 1 + \omega(\lambda_i' - 1)$, where the λ_i' are the eigenvalues of T' , and which has the same eigenvectors. We used $\omega = 2$, which works well in practice.

IV. PARALLEL PROCESSING APPROACH

The reduced transition matrix for $L = 15$ contains about 10^8 elements, so both computational cost (10 Tf ops for 50,000 iterations) and memory requirements (1.6 Gbyte) are too high for regular workstations or PCs. We used the parallel programming library BSPlib [20] to obtain our results on a Cray T3E supercomputer, using up to 64 processors. Within the Bulk Synchronous Parallel (BSP) computing model [21], computations and interprocessor communications are separated by global synchronizations. BSPlib supports two types of communication: direct remote memory access (DRMA) and bulk synchronous message passing (BSMP). The DRMA operation **put** copies data into the memory space of a remote processor at the next synchronization, and **get** retrieves data from a remote processor at the next synchronization. The BSMP operation **send** sends a packet to a queue on a remote processor, which, after the next synchronization, can be accessed there with the **move** operation. In total, the BSP library has 20 primitives. We use the most efficient primitive, **put**. This can be done because the matrix remains constant during all the iterations, so that it becomes worthwhile to analyze the communication pattern beforehand and to store a list of memory addresses to be used as the target of **put** operations.

In our problem, for $L > 12$, we cannot afford to store the complete matrix on a single processor, so we need to distribute it over a number of processors. The traditional way to do this is to distribute blocks of rows of the matrix over the processors (even though for dense matrices and certain sparse matrices it has been shown that this is not the most efficient way for communication [22]). In principle, we use a more general, two-dimensional matrix distribution, which we will tailor to our problem. The general computation of a matrix–vector product $\vec{x}' = A\vec{x}$ with communication is as follows. The matrix and vector are distributed over the processors: the nonzero matrix elements A_{ij} and the vector components x_j are each assigned to a processor. The matrix–vector product is given by $x'_i = \sum_j A_{ij}x_j$. The first step is to communicate the components x_j to the processors with the corresponding A_{ij} . Now, each processor q computes the partial row sums $s_{iq} = \sum'_j A_{ij}x_j$, where \sum'_j denotes a summation that runs only over indices j for which A_{ij} has been assigned to processor q . The partial row sums are then communicated to the processor containing x'_i , and finally they are accumulated into the components x'_i .

The matrix we have to deal with is sparse and we exploit this in our computations, since we only handle nonzero elements A_{ij} . In addition, the nonzero structure shows “patches” with many nonzero elements. We can exploit this to make our communications faster. Consider a rectangular patch (i.e., a contiguous submatrix). A value x_j must be sent to the owner of the patch if an element A_{ij} in column j of the patch is nonzero. It is likely that most columns of the patch have at least one nonzero, so we might as well send all x_j for that patch. This makes it possible to send a contiguous subvector of \vec{x} , which is more efficient than sending separate components; this comes at the expense of a few unnecessary communications. The trade-off can be shifted by increasing or decreasing the patch size.

To find suitable patches, we first divide the state vector into contiguous subvectors. We use a heuristic to partition the matrix into blocks of rows with approximately the same number of nonzeros. If we use P processors, and we want each processor to have K subvectors, we have to divide the vector into KP subvectors. (The factor K is the overpartitioning factor.) This initial division tries to minimize the computation time. Next, we adjust the divisions to reduce communication: a suitable patch in the matrix corresponds to an input subvector of kink representations where only the last few bits differ, and also to an output subvector with that property. Therefore, we search for a pair of adjacent kink representations that has a different bit as much as possible to the left. This is a suitable place to split. We try to keep the distance from the starting point as small as possible.

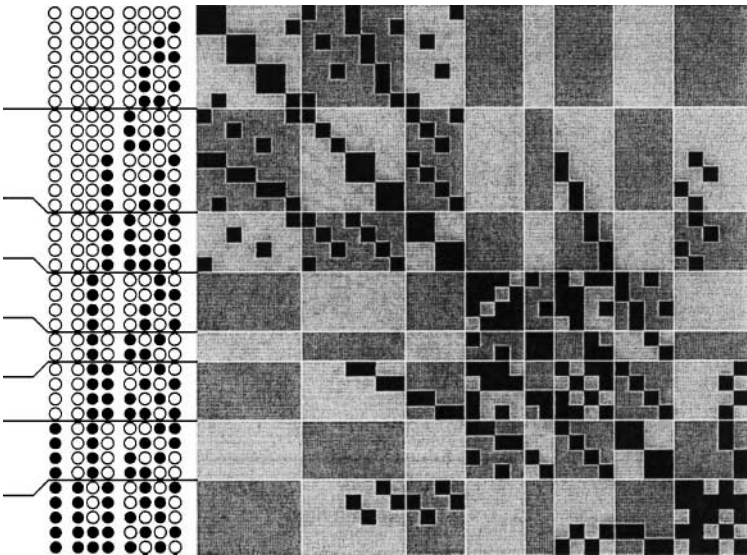


FIG. 4. Reduced transition matrix for polymer length $L = 5$. The size of the matrix is 37×37 and it has 233 nonzero elements, shown as black squares. To the left of each row is the corresponding kink representation written as a binary number, with black circles denoting 1 and open ones 0. The horizontal lines on the left show the initial division of the reduced state vector into eight contiguous parts, optimized to balance the number of nonzeros in the corresponding matrix rows. The jumps of these lines indicate slight adjustments to make the division fit the nonzero structure of the matrix. The resulting vector division induces a division of the rows and columns of the matrix, and hence a partitioning into 64 submatrices, shown by the gray checkerboard pattern. Complete submatrices are now assigned to the processors of a parallel computer.

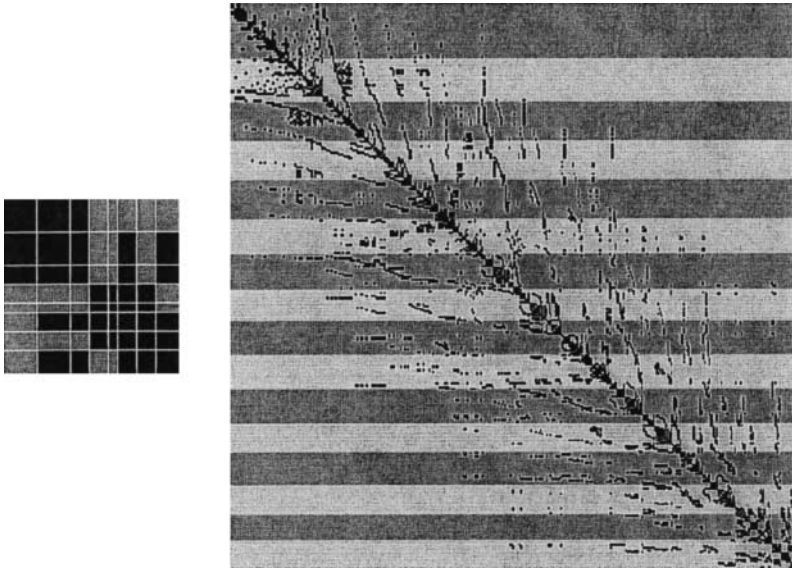


FIG. 5. Communication matrix for $L = 5$ (left) and $L = 13$ (right). Note that the matrix for $L = 5$ can be obtained by replacing each nonempty submatrix in Fig. 4 with a single nonzero element. The communication matrix for $L = 13$, of size 320×320 , is distributed over 16 processors in a row distribution.

As an example of the structure of the reduced transition matrices and the division into submatrices, we show the nonzero structure of the matrix for $L = 5$ in Fig. 4 and its corresponding communication matrix in Fig. 5 (left). The communication matrix is built from the partitioned transition matrix by considering each submatrix as a single element. It is a sparse matrix of much smaller size which determines the communication requirements. Our communication matrix for $L = 13$ is given in Fig. 5 (right).

V. RESULTS: DRIFT VELOCITIES AND DIFFUSION COEFFICIENTS

Figure 6 shows the numerically exact values for the drift velocity of the cage polymers up to length $L = 15$. As expected, initially the drift velocity increases linearly with field strength, and eventually it reaches a maximum drift velocity, after which it decreases exponentially with field strength. Clearly visible in Monte Carlo data [19] is a regime just before the maximum velocity where the drift velocity increases quadratically with the field strength; in the numerically exact data presented here, for relatively short chains, this regime is invisible.

The diffusion coefficient is computed from the drift velocities using the Nernst–Einstein relation $v = qLED$, which holds for vanishing E . We used the computed velocities in the range $E = 10^{-6}$ to 10^{-3} to fit a second-order polynomial to the mobility $\mu = v/E$ of the polymers (see Table II). The relative statistical error in the mobility found by the fitting procedure was about 10^{-9} .

It is known that asymptotically for large polymers the diffusion coefficient behaves as $D \sim L^{-2}$, but with large finite-size corrections for usual polymer lengths. As the polymers are modeled as a random walk of $N = L - 1$ steps, finite-size corrections of the order of $N^{-1/2}$ are expected. Let us call $d(N) = D \cdot (N + 1)^2 = DL^2$, and $d_\infty = (DL^2)_{L \rightarrow \infty}$;

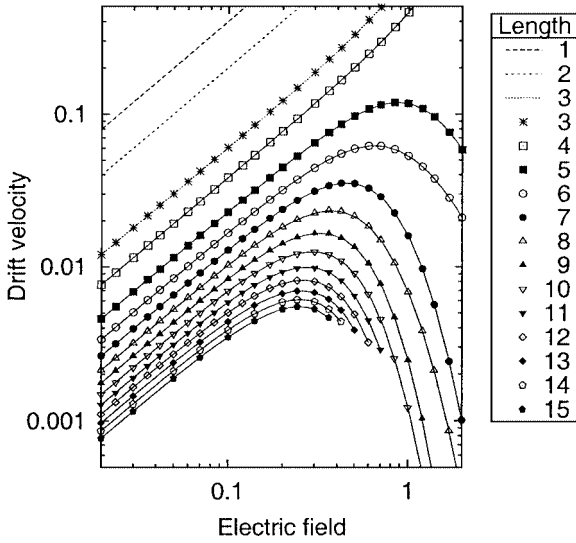


FIG. 6. The graphs show the computed drift velocities of the cage polymers as a function of electric field strength E . For $E \leq 1$, the relative error is less than 10^{-10} , all other points have a relative error less than 10^{-4} . The graphs for lengths 1, 2, and 3 are $v_1 = 2(e^E - e^{-E})$, $v_2 = e^E - e^{-E}$, and $v_3 = 4(e^{3E} - e^{-3E})/(18 + 11(e^{2E} + e^{-2E}))$, respectively; for $L > 3$, the computed points are connected by straight lines.

we expect that for large but finite polymers $d(N) = d_\infty + aN^{-x}$. The parameters a and x can be found from this equation by differentiation: $\frac{\partial d}{\partial N} = -aN^{-x-1} \approx \frac{1}{2}(d(N+1) - d(N-1))$. A least-squares fit of the derivative of the new data against N for $N = 8-13$ gives $a = 2.469(5)$ and $x = 0.512(6)$, strongly suggesting finite-size corrections with an

TABLE II
Diffusion Coefficients for Cage Polymers up to Length
 $L = 15$, Obtained by a Second-Order Polynomial Fit to the
Mobility for Field Strengths in the Range $[10^{-6}, 10^{-3}]$

| L | D | $L^2 D$ |
|-----|----------------|--------------|
| 3 | 0.200000000000 | 1.8000000000 |
| 4 | 0.095541401266 | 1.5286624203 |
| 5 | 0.045892037845 | 1.1473009461 |
| 6 | 0.028134332038 | 1.0128359534 |
| 7 | 0.018844680457 | 0.9233893424 |
| 8 | 0.013302014727 | 0.8513289425 |
| 9 | 0.009776090804 | 0.7918633551 |
| 10 | 0.007424928047 | 0.7424928047 |
| 11 | 0.005790292327 | 0.7006253716 |
| 12 | 0.004615107027 | 0.6645754118 |
| 13 | 0.003746569186 | 0.6331701925 |
| 14 | 0.003089624043 | 0.6055663124 |
| 15 | 0.002582785984 | 0.5811268465 |

Note. An upper bound for the relative error is 10^{-9} . For long polymers, $L^2 D$ converges to a constant [18].

exponent $\frac{1}{2}$. This shows an advantage of the numerically exact computations over Monte Carlo simulations in that we can compute the derivative of the data reliably.

We used our new diffusion coefficients, combined with data from Refs. [18, 19], to find the length dependence of the diffusion coefficient. A least-squares fit with $d(N) = a + bN^{-1/2} + cN^{-1}$ gives $d(N) = 0.172(6) + 0.63(8)N^{-1/2} + 3.3(2)N^{-1}$, and a least-squares fit with $d(N) = (a' + b'N^{-1/2} + c'N^{-1})^{-1}$ gives $d(N) = (5.67(5) - 22.2(5)N^{-1/2} + 28(2)N^{-1})^{-1}$. Both of these expansions converge, within the error margins, to the same value for large N . The first expansion converges to 0.172(6), and the second expansion converges to $1/5.67(5) = 0.176(2)$. Combining these results, we conclude that for large L the diffusion coefficient is $D = 0.175(2)L^{-2}$. Our diffusion coefficient agrees with that of Barkema and Krenzlín [18], but they reported a different finite-size scaling: $DN^2 = 0.173 + 1.9N^{-2/3}$.

VI. RESULTS: COMPUTATION TIME AND EFFICIENCY

Our computations were performed on a Cray T3E computer. The peak performance of a single node of the Cray T3E is 600 Mfop/s for computations. The `bsp_probe` benchmark shows a performance of 47 Mfop/s per node [20]. The peak interprocessor bandwidth is 500 Mbyte/s (bidirectional). The `bsp_probe` benchmark shows a sustained bidirectional performance of 94 Mbyte/s per processor when all 64 processors communicate at the same time. This is equivalent to a BSP parameter $g = 3.8$, where g is the cost in flop time units of one 64-bit word leaving or entering a processor. The measured global synchronization time for 64 processors is 48 μ s, which is equivalent to $l = 2259$ flop time units.

Table III presents the execution time of one iteration of the algorithm in two forms: the BSP cost $a + bg + cl$ counts the flops and the communications and thus gives the time on an arbitrary computer with BSP parameters g and l , whereas the time in milliseconds gives the measured time on this particular architecture, split into computation and communication time. (The total measured synchronization time is negligible). The BSP cost can be used to predict the run time of our algorithm on different architectures. Table III also gives the efficiency and speedup relative to a sequential program.

Peak computation performance is often only reached for dense matrix–matrix multiplication; the performance for sparse matrix–vector multiplication is always much lower. Comparing the flop count and the measured computation time for the largest problem $L = 15$, we see that we achieve about 10.5 Mfop/s per processor. Comparing the communication count with the measured communication time, we obtain a g -value of 8.1 μ s (or $g = 3.8$ flop units; see above). This means that we attain the maximum sustainable

TABLE III
BSP Cost, Time, Efficiency, and Speedup for One Matrix–Vector Multiplication

| L | P | BSP cost | Time (ms) | Efficiency | Speedup |
|-----|-----|-------------------------------|-------------|------------|---------|
| 12 | 8 | $545,156 + 64,716g + 2l$ | $47 + 4.3$ | 85% | 6.8 |
| 13 | 16 | $1,002,824 + 187,347g + 2l$ | $89 + 13$ | 81% | 13.0 |
| 14 | 32 | $1,836,920 + 425,152g + 2l$ | $169 + 44$ | 73% | 23.4 |
| 15 | 64 | $3,452,776 + 1,380,415g + 2l$ | $330 + 112$ | 67% | 42.9 |

communication speed. This is due to the design of our algorithm, which communicates contiguous subvectors instead of single components. Furthermore, the results show that our choice of optimizing mainly the computation (by choosing a row distribution) is justified for this architecture: the communication time is always less than a third of the total time. For a different machine, with a higher value of g , more emphasis must be placed on optimizing the communication, leading to a two-dimensional distribution.

Each iteration of our computation contains one matrix–vector multiplication. The number of iterations needed for convergence depends on the length of the polymer, and on the applied electric field. The iteration was stopped when either the accuracy was better than 10^{-10} or the number of iterations exceeded 100,000. In the latter case, the accuracy was computed at termination. Typically, for $L = 15$ and a low electric field strength, 50,000 iterations are needed. Only computed values with accuracy 10^{-4} or better are shown in Fig. 6. For $L = 12$, we compared the output for the parallel program with that of the sequential program and found the difference to be within rounding errors. The total speedup for $L = 15$, compared to a naive implementation (for which one would need 38.5 Tbyte of memory), is a factor 1.5×10^6 : a factor of 17,248 by using a reduced state space, a factor of 2 by shifting the eigenvalues of the reduced transition matrix, and a factor of 42.9 by using a parallel program on 64 processors.

VII. CONCLUSIONS

In numerically exact computations on the cage model, extended for the study of DNA electrophoresis, we exploited symmetries of the model, improved the eigenspectrum of the transition matrix, and applied parallel processing. This has resulted in a computational speedup factor of over a million.

Regarding the cage model, we conclude that the polymer diffusion coefficient D scales asymptotically for large polymers as $DL^2 = 0.175(2)$, in qualitative agreement with de Gennes’ reptation arguments, and in quantitative agreement with earlier simulation reports [18]. The finite-size corrections are found to be a combination of $N^{-1/2}$ (which asymptotically is the dominant correction) and N^{-1} , and probably higher order corrections; this is in disagreement with earlier reports [11, 18], where the leading corrections were reported to be $N^{-2/3}$, but in agreement with recent density matrix renormalization group computations by Carlon *et al.* [23].

APPENDIX: CORRECTNESS PROOF OF KINK REPRESENTATION APPROACH

Our aim is to prove that all polymer configurations with the same kink representation have the same probability in the steady state. It is sufficient to show that two configurations with the same kink representation can move to the same set of six kink representations with the moving of a certain kink or end monomer. We prove this by giving a procedure for determining the resulting six kink representations.

First, we introduce our notation. Define $R(i, j)$ as the statement “the part of the configuration between monomers i and j is removable,” where $0 \leq i, j < L$. (By this definition, $R(i, i)$ holds.) Define $S(i, j)$ as “monomers i and j are at the same site.” Define $\text{sign}(i) = 1$ if bond $[i, i + 1]$ is in the direction of the electric field, and $\text{sign}(i) = -1$ otherwise. We have the following useful properties.

1. $R(i, j)$ implies $S(i, j)$ and $j - i$ even.
2. Let $i < j < k$. If $R(i, k)$ and j is the center of a kink, then the part between i and k can be removed, starting with the kink at j . Proof: By induction on the length of the part.
3. The relations R and S are equivalence relations between monomers, i.e., they are reflexive, symmetric, and transitive. Proof: Trivial, except for the proof of the transitivity of R , which uses the previous property. For example, let $i < j < k$. If $R(i, k)$ and $R(i, j)$, then a removal of the part $[j, k]$ can be obtained by starting the removal of $R(i, k)$ by removing kinks in $[i, j]$.
4. Let j be the smallest integer such that $j > i$ and $R(i, j)$. Then $R(i + 1, j - 1)$. Proof: By induction on the length of $[i, j]$.
5. Let i, i', j, j' be monomers with $|i - i'| = |j - j'| = 1$. If $R(i, j)$ and $S(i', j')$, then $R(i', j')$. Proof: We treat the case $i' = i + 1$ and $j' = j + 1$ as an example. First, we extend the part $[i, j]$ with a dummy monomer $i - 1$ at the site of i' . We can remove $[i - 1, j]$ by first removing $[i, j]$ and then removing the remaining kink $[i - 1, j]$. According to Property 2 above, we can also start with kink $[i - 1, i']$ and then remove $[i', j']$. Hence $R(i', j')$.

Now assume that the kink at i of a given polymer configuration moves. (Moves of end monomers can be treated similarly.) We present a procedure for generating the resulting six kink representations, which is based solely on the original kink representation, i.e., on the relation R and the bond signs. The correctness proof of this procedure uses the properties above; for brevity, we omit the details. A kink exists at i if and only if $R(i - 1, i + 1)$. In that case, $\text{sign}(i) = -\text{sign}(i - 1)$. The set of removable parts $[x, y]$ with $x, y \neq i$ does not change; changes can only occur if $x = i$ or $y = i$. The procedure checks for all j whether $R(i + 1, j)$. If so, monomer i can move to the sites of monomers $j - 1$ and $j + 1$, provided these monomers exist. This is because $j - 1, j + 1$, and i are all at distance one from the site of j . If $j - 1 = i$, then $R(i + 1, j)$ holds, and the move to $j - 1$ is the identity move, which does not change the kink representation. Assume the move is to $j - 1$ (the case $j + 1$ is similar). Assume $j - 1 \neq i$. The new set of $x \neq i$ with $R(i, x)$ equals the old set of $x \neq i$ with $R(j - 1, x)$. The new $\text{sign}(i)$ equals the old $\text{sign}(j - 1)$.

The generated moves are collected and duplicates are removed by using the old relation R . For example, if $R(i + 1, j)$ and $R(i + 1, j')$ and we have to check whether moves to $j - 1 \neq i$ and $j' - 1 \neq i$ are identical, i.e., whether $S(j - 1, j' - 1)$, we can do this by checking the old $R(j - 1, j' - 1)$. The total number of moves after duplicate removal is at most six. To make the total six, extra moves are added. This is done such that three moves have $\text{sign}(i) = 1$ and the others $\text{sign}(i) = -1$. The relation R after such an extra move is the same as before the moves, except that $R(i, x)$ becomes false for all $x \neq i$. Note that $R(i, x)$ with $x > i$ implies that there exists a smallest $x' > i$ with $R(i, x')$, and this in turn implies $R(i + 1, x' - 1)$, so that the corresponding move of i to x' must have been generated previously.

ACKNOWLEDGMENTS

We would like to thank the Dutch National Computer Facilities foundation and the High Performance Applied Computing center at Delft University of Technology for providing access to a Cray T3E.

REFERENCES

1. P. G. de Gennes, Reptation of a polymer chain in the presence of fixed obstacles, *J. Chem. Phys.* **55**, 572 (1971).

2. M. Rubinstein, Discretized model of entangled-polymer dynamics, *Phys. Rev. Lett.* **59**, 1946 (1987).
3. J. M. J. van Leeuwen and A. Kooiman, The drift velocity in the Rubinstein-Duke model for electrophoresis, *Physica A* **184**, 79 (1992).
4. A. Kooiman and J. M. J. van Leeuwen, Reptation models for electrophoresis, *Physica A* **194**, 163 (1993).
5. A. Kooiman and J. M. J. van Leeuwen, The drift velocity in reptation models for electrophoresis, *J. Chem. Phys.* **99**, 2247 (1993).
6. M. Prähofer and H. Spohn, Bounds on the diffusion constant for the Rubinstein-Duke model of electrophoresis, *Physica A* **233**, 191 (1996).
7. T. A. J. Duke, Tube model of field-inversion electrophoresis, *Phys. Rev. Lett.* **62**, 2877 (1989).
8. T. A. J. Duke, Monte-Carlo reptation model of gel-electrophoresis: steady state behavior, *J. Chem. Phys.* **93**, 9049 (1990).
9. T. A. J. Duke, Monte-Carlo reptation model of gel-electrophoresis: response to field pulses, *J. Chem. Phys.* **93**, 9055 (1990).
10. B. Widom, J. L. Viovy, and A. D. Defontaine, Repton model of gel-electrophoresis and diffusion, *J. Phys. I France* **1**, 1759 (1991).
11. G. T. Barkema, J. F. Marko, and B. Widom, Electrophoresis of charged polymers: simulation and scaling in a lattice model of reptation, *Phys. Rev. E* **49**, 5303 (1994).
12. T. A. J. Duke, A. N. Semenov, and J. L. Viovy, Mobility of a reptating polymer, *Phys. Rev. Lett.* **69**, 3260 (1992).
13. G. T. Barkema and M. E. J. Newman, The repton model of gel electrophoresis, *Physica A* **244**, 25 (1997).
14. M. E. J. Newman and G. T. Barkema, Diffusion constant for the repton model of gel electrophoresis, *Phys. Rev. E* **56**, 3468 (1997).
15. G. T. Barkema, C. Caron, and J. F. Marko, Scaling properties of gel electrophoresis of DNA, *Biopolymers* **38**, 665 (1996).
16. A. Kolomeisky, *One-Dimensional Nonequilibrium Stochastic Models, Interface Models, and Their Applications*, Ph.D. thesis (Cornell University, Ithaca, New York, 1998).
17. K. E. Evans and S. F. Edwards, Computer simulation of the dynamics of highly entangled polymers, *J. Chem. Soc. Faraday Trans. 2* **77**, 1891 (1981).
18. G. T. Barkema and H. M. Krenzlín, Long-time dynamics of de Gennes' model for reptation, *J. Chem. Phys.* **109**, 6486 (1998).
19. A. van Heukelum and H. R. W. Beljaars, Electrophoresis simulated with the cage model for reptation, *J. Chem. Phys.* **113**, 3909 (2000).
20. J. M. D. Hill, B. McColl, D. C. Stefanescu, M. W. Goudreau, K. Lang, S. B. Rao, T. Suel, T. Santilas, and R. H. Bisseling, BSPlib: The BSP programming library, *Parallel Comput.* **24**, 1947 (1998).
21. L. G. Valiant, A bridging model for parallel computation, *Commun. ACM* **33**(8), 103 (1990).
22. R. H. Bisseling and W. F. McColl, Scientific computing on bulk synchronous parallel architectures, in *Proc. IFIP 13th World Computer Congress* (North-Holland, Amsterdam, 1994), Vol. 1, p. 509.
23. E. Carlon, A. Drzewiński, and J. M. J. van Leeuwen, Crossover behavior for long reptating polymers, *Phys. Rev. E* **64**, 010801 (R) (2001).